Journal of Applied Sciences and Nanotechnology, Vol. 3, No. 3 (2023)

Journal of Applied Sciences and Nanotechnology

Journal homepage: jasn.uotechnology.edu.iq

Characterisation of Prepared Polyaniline Nanofibers Based on a Hydrothermal Variation of Aniline Concentration

[1,2]Sura R. Mohammed*, [2]Mukhlis M. Ismail, [3]Isam M. Ibrahim

[1]Iraqi National Monitoring Authority, Ministry of Science and Technology – Iraq
[2]Department of Applied Sciences, University of Technology – Iraq
[3]Departments of Physics, College of Science, University of Baghdad – Iraq

ARTICLE INFO

Article history:
Received: February, 03, 2023
Accepted: July, 26, 2023
Available online: September, 10, 2023

Keywords:
Polyaniline,
Hydrothermal method,
Nanofibers

Corresponding Author:
Sura R. mohammed
surar9189@gmail.com

ABSTRACT

Polyaniline nanofibers (PAni-NF_s) have been synthesised under various concentrations (0.12, 0.16, and 0.2 g/L) of aniline and different times (2h and 3 h) by hydrothermal method at 90°C. Was conducted with the use of X-ray diffraction (XRD), Fourier Transform Infrared spectra (FTIR), Ultraviolet-Visible (UV-VIS) absorption spectra, Thermogravimetric Analysis (TGA), and Field Emission-Scanning Electron Microscopy (FE-SEM). The X-ray diffraction patterns revealed the amorphous nature of all the produced samples. FE-SEM demonstrated that polyaniline has a nanofiber-like structure. The observed typical peaks of PAni were (1580, 1300-1240, and 821 cm^{-1}), analysed by the chemical bonding of the formed PAni through FTIR spectroscopy. Also, tests indicated the promotion of the thermal stability of polyaniline nanocomposite at temperatures above 600°C. Still, the PAni-0.12 g/L sample was better than the other samples, and the optical parameters manifested a decrease in the band gap (E_g) band gap. The observed TGA test findings also promoted polyaniline's thermal stability at temperatures reaching 600°C.

https://doi.org/10.53293/jasn.2023.6439.1204, Department of Applied Sciences, University of Technology - Iraq.

1. Introduction

The conductivity of some polymers has been recognised for a very long time. Different types of conductive polymers are commercially accessible. They include polythiophene (PTh), polycarbazole, polypyrrole (PPy), and polyaniline (PAni) [1]. An inherently conducting polymer is any polymer that retains its mechanical qualities while exhibiting the electrical, electronic, and optical characteristics of metals. Interesting electric conductivity, optical, and electro-activity properties are present in the conducting polymers, including polyaniline [2]. The conducting polyaniline (PAni), composed of benzenoid and quinonoid units with delocalised conjugated structures, has several redox states, which have become the research focus in conducting polymers [3, 4]. The conductivity and processability of PAni can be adjusted by selecting a suitable dopant and varying oxidation states [5]. Polyaniline (PAni) has attracted great attention because of its easy synthesis pathway, relative environmental and thermal stability, high electrical conductivity, [6, 7] relatively low cost [8] and a wide range of applications, such as secondary batteries [9], solar cells [10], corrosion devices [11], organic light emitting diodes [12], bio-chemical sensors [13], and supercapacitors [14]. Additionally, the electrical, aeronautical, gas sensing, and military industries. However, due to their introduction to the market and new applications, there has been an improvement in the actual application of these compounds in recent years. [15]. Conductive polymers are inexpensive, lightweight, and, more recently, straightforward to manufacture [16]. There are several methods for preparing polyaniline, including the chemical oxidation method, the electropolymerisation of aniline, and the hydrothermal synthesis method. The latter method was used to form tiny micro or nanoparticles at a low cost compared to other methods that require complex devices and tools at a high cost [17]. Many studies on polyaniline have shown that its chemical and physical properties strongly depend on the method of preparation and the composition of the solution through the difference in the concentration of aniline. The polyaniline nanostructures can be controlled, and there are different types of them (i.e., nanotubes, -rods, -fibres, and -wires) [18]. In this work, three PAni Concentrations (0.12, 0.16, and 0.2 g/L) have been prepared by hydrothermal method to study their properties utilising PAni to create PAni nanofibers to improve the qualities of PAni. These powders were investigated for their structural, morphological and optical properties

2. Experiments Section

2.1 Used Material

Aniline monomer (Ani) (99.6%, India CDH, Ltd), Ammonium Persulphate (APS) $(NH_4)_2S_2O_8$ (99.8%, India CDH, Ltd), hydrochloric acid (HCl) (99.8%, India CDH, Ltd) Deionised water, and ethanol were used in the present work.

2.2 Preparation of Polyaniline

Aniline was dissolved into 76 mL of deionised water and stirred using a magnetic stirring device for 20 minutes at room temperature. Then 0.217 g of Ammonium Persulphate (APS) was added to 4 mL of distilled water while stirring continuously for 20 minutes at room temperature. After that, the aniline solution was mixed with the APS solution, and 1.4 mL of HCl was added drop by drop to the resulting solution. The final solution was put in a 100 mL Teflon-lined autoclave reactor and stainless steel. The autoclave was heated at 90°C in an electronically controlled temperature oven for approximately two to three hours. The autoclave was then quickly and easily cooled in an ice bath. The precipitate was centrifuged and rates 2000 cycles for 10 min rinsed with water and ethanol, respectively, until the liquid became colourless, then followed by drying for 4 hours at 60°C in an oven to obtain the PAni powder.

2.3 Characteristics

In this investigation, the purity and crystalline quality of the phase were examined using a powdered X-ray patterns instrument (Shimadzu 6000). The conditions for measurement were as follows: Target (CuK), wavelength: (1.54), Voltage (40 kV), Current (mA), Scan Angle (5-70°), and Scan Speed (°/min). Shimadzu, a Japanese manufacturer, provided the FTIR utilising IR Affinty-1 CE (FTIR) spectrophotometer. This method has a resolution of (0.5 cm^{-1}) and operates in the (4000-500 cm^{-1}) wave number range. The specimen's morphology was examined using a Zeiss Ultra plus 55 FE-SEM. The UV-VIS 1800 Double Beam Spectrophotometer, manufactured by the Japanese company Shimadzu, was used to measure the surface area value and pore size distributions. By putting a similar solution in the reference beam, the transmission of the solution was recorded.

3. Results and Discussion

3.1. Scanning Electron Microscopy with Field Emission (FE-SEM)

PAni surface morphologies at different aniline concentrations (0.12, 0.16, and 0.2 g/L) and for two periods of time (2 h and 3 h) evinced nanofiber-like surface morphologies; this agrees with the research [19]. In Fig. 1a, 1b, and 1c under the conditions of 90°C temperature for 2 h and aniline concentration (0.12 g/L), the results showed the formed PAni nanofibers with a diameter range of ~ 52-76 nm and for (0.16 g/L) a diameter range of ~ 71-83 nm. However, as the concentration of (0.20 g/L) was increased, the size of PAni nanofibers range increased to ~52-105 nm, respectively. In Fig. 1d, 1e and 1f at temperature 90°C for 3 h and aniline concentration (0.12 g/L), the results elucidated the formed PAni nanofibers with a diameter range of ~ 33-55 nm and for (0.16 g/L) a diameter range of ~ 47-66 nm. Nevertheless, as the concentration of (0.2 g/L) was raised, the size of the PAni nanofiber range reached ~ 47-73 nm, respectively; this means that the diameter range increases by increasing the aniline concentration and decreases by increasing the time in the oven [20]. Such successful formation of nanofibers is like the morphology of PAni [21]. By examining the SEM of the polyaniline material prepared at a temperature of

90°C and different concentrations (0.12, 0.16, and 0.2 g/L) of aniline and two times (2 and 3 h) in the oven, the best results were determined at 90°C for 3 h and approved to complete the research examinations.

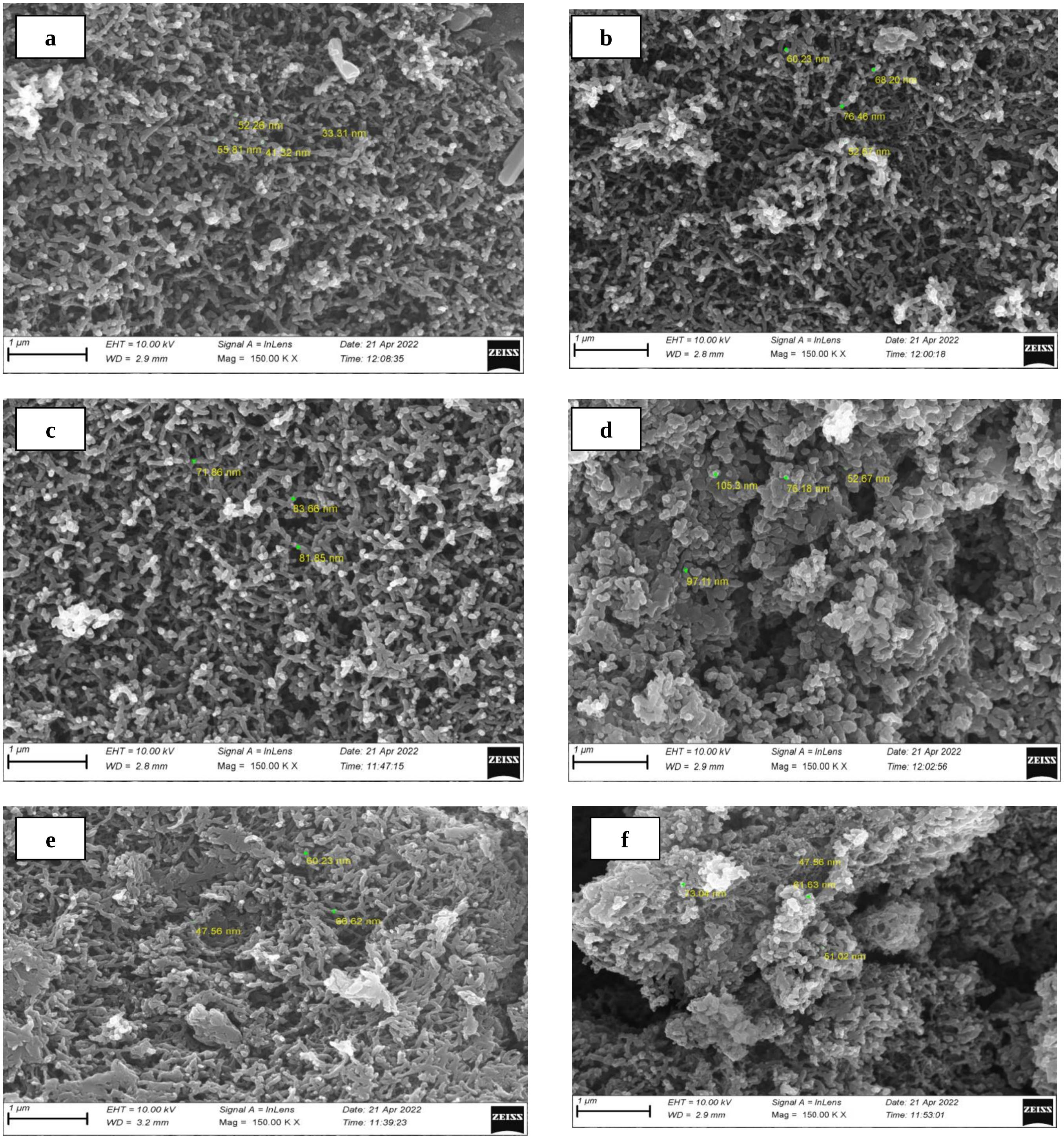

Figure 1: Polyaniline nanofibers in the presence of different aniline concentrations: (a) 0.12 g/L, (b) 0.16 g/L, (c) 0.2 g/L at 90°C for 2h, and (d) 0.12 g/L, (e) 0.16 g/L, (f) 0.2 g/L at 90°C for 3h.

3.2 X-Ray Diffraction (XRD)

Type X-ray diffraction pattern equipment was utilised to investigate the structural properties of PAni-NFs generated by hydrothermal technique for 3 hr at a temperature (90°C). As displayed in Fig. 2, the XRD patterns of all samples have an amorphous background that agrees with references [22, 23]. The pattern of PAni demonstrates a broad diffraction peak at $2\theta = 20°$ corresponding to the periodicity perpendicular and parallel to the chains of PAni, which confirms the amorphous nature of PAni. The peak at $2\theta = 20°$ also exhibits the characteristic distance between the ring planes of benzene rings in adjacent chains or the close-contact inter-chain space [21].

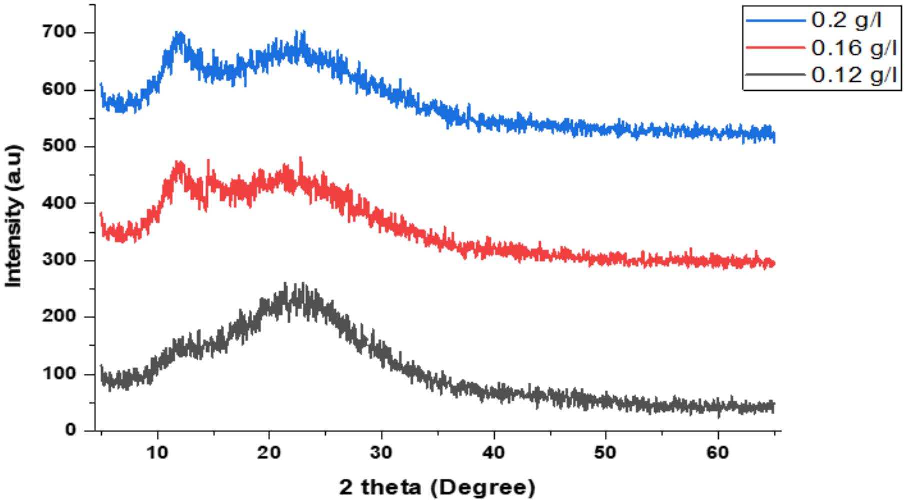

Figure 2: XRD pattern of PAni NFs.

3.3 Fourier-Transform Infrared Spectroscopy (FTIR)

Double-beam Fourier transforms infrared was utilised to record the IR transmission spectra. Fig. 3 depicts the spectra of PAni produced through the hydrothermal technique. The major peaked sites of each PAni are essentially similar; a broad band at (3448 cm^{-1}) is due to the (N–H) stretching vibrations resulting from the protonation of nitrogen.

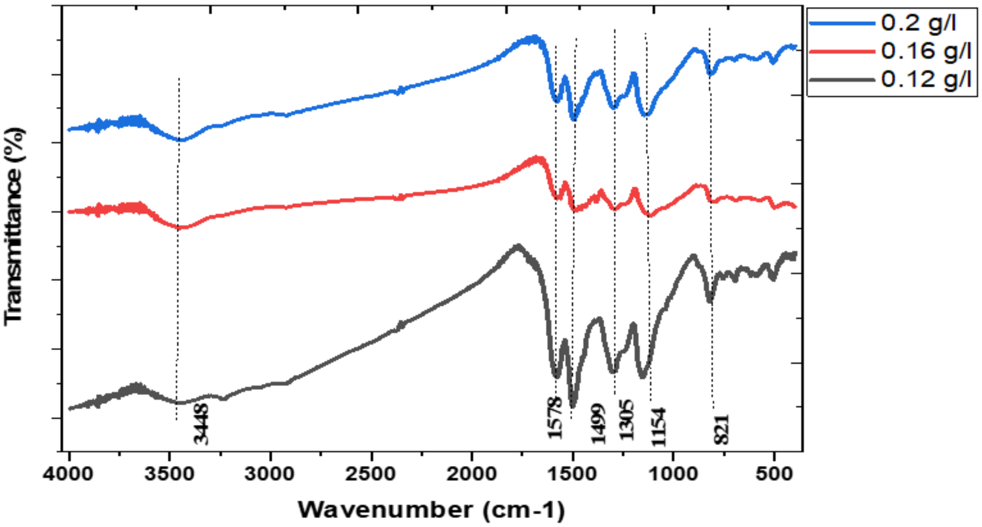

Figure 3: FTIR of PAni different aniline (0.12, 0.16 and 0.2 g/L) concentrations.

The two bands at (1566–1579 cm^{-1}) and (1488–1498 cm^{-1}) correspond to the stretching vibrations of the (C=N) quinoid and (C=C) benzenoid rings, respectively, agree with the research [23]. The peak at (1488 cm^{-1}) and (1579 cm^{-1}) is attributed to the (C=N) and (C=C) stretching vibrations between benzenoid and quinoid units. In contrast, the absorption peak arises at (821 cm^{-1}), which corresponds to the (C-C) and (C-H) vibration bands of the benzenoid ring. The band at (1297–1311 cm^{-1}) may be (C-N-C) stretching vibration, while the peak at (1297 cm-

^{1}) is owing to the distinctive absorption band for the (C–N) stretching mode, attributable to the aromatic amine structure of the polymers. The absorption peak at 3448 cm^{-1} is associated with the vibration band (N-H) of polyaniline, and these results are consistent with the findings of the research [24], confirming that the aniline polymerisation was successful.

3.4 UV-Visible Spectrophotometer Results

Employing a spectrometer (UV–VIS 1800 Double beam spectrophotometer), the optical transmission and absorption spectra of inorganic–polyaniline solutions in the visible and NIR (200–1000 nm) bands were examined. Fig. 4 portrays the transmission spectrum of PAni between 200 and 1000 nm. It is clear that the transmittance grows fast within the wavelength range of (310-600 nm) but then tends to increase gradually at higher wavelengths. The spectrum illustrates an increased transmittance in the visible and infrared ranges but a poor transmittance in the ultraviolet region [25]. Additionally, the fundamental absorption edge in the visible part of the spectrum is sharp. Furthermore, the vital absorption edge is shown to be sharp in the visible range at a wavelength of (685 nm).

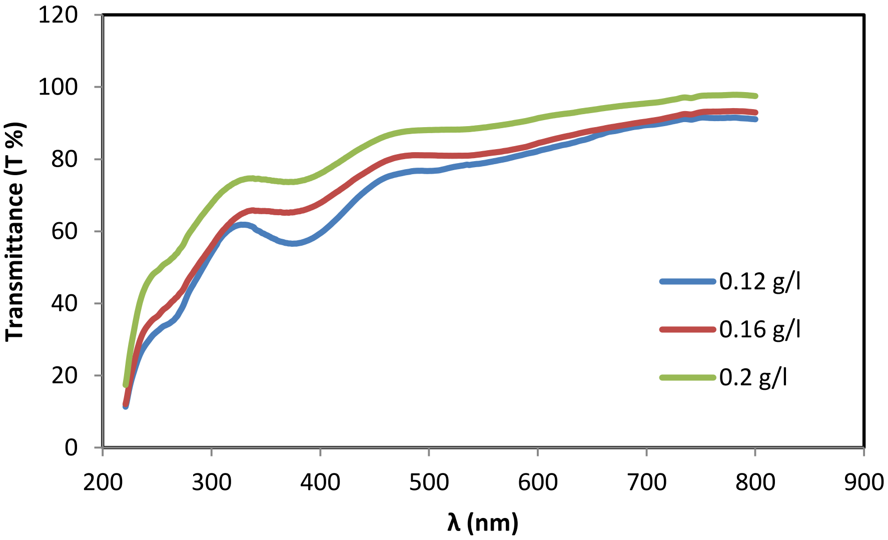

Figure 4: Transmittance vs wavelength (λ) of PAni NFs.

The absorption spectrum is the most important method for evaluating the optical energy gap (Eg) of inorganic and organic semiconductors [26]. The energy gap, also known as the band gap, is relevant since it controls the electrical conductivity and optical absorption of PAni. The absorption coefficient (α) is determined using Beer Lambert's relation = 2,303 A/l, where A is the absorbance, and l is the path length [23, 24]. The absorption coefficient of PAni as a function of its wavelength is seen in Fig. 5. In several amorphous materials, the photon absorption conforming to the Tauc equation (Eq. (1)) [27] is an equation of the following form:

$$\alpha h\nu = A(h\nu - E_g)^n \qquad (1)$$

Where (hυ) is the energy of the input photon, (A) is the disordered parameter, (E_g) is the optical energy band gap, and (n) is the power coefficient. The values for indirect and direct allowed transitions are 1/2 and 2, respectively [24]. For a high absorption coefficient, > 103 cm^{-1}, which relates to a direct transition, the index n = 1/2 defines the energy gap permitted for the direct transition. (hυ)^{2} graphs are used to calculate the energy gap.

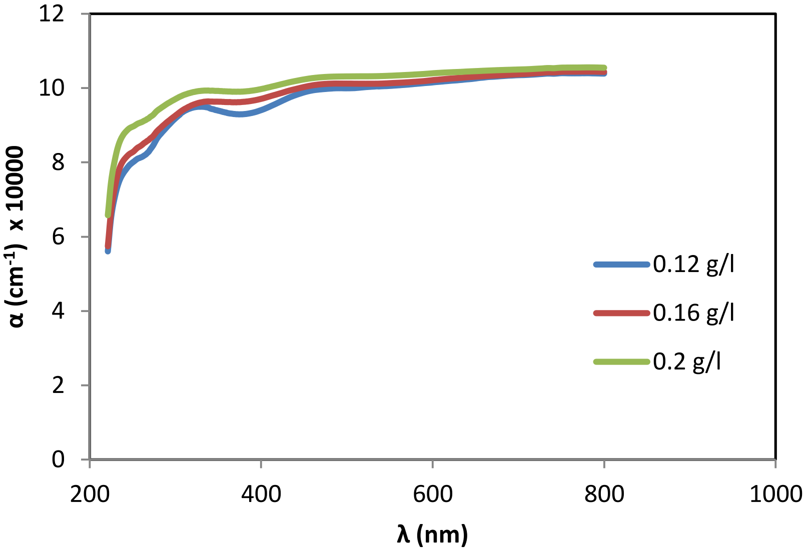

Figure 5: Polyaniline absorption index as a function of wavelength.

According to Fig. 6, The optical energy gap values for all the prepared samples were calculated using Eq. 1 when the constant value (1/2 = r). By drawing the relationship between (αhν) and the energy of the incident photon (hν) and by drawing a tangent to the straight part of the curve to cut the photon energy axis (αhν), as this point of intersection represents the value of the energy gap for the allowed direct transitions, as the binding energies of pure PAni with (0.2, 0.16, and 0.12 g/L) are (2.25, 2.38, and 2.82 eV), respectively. The possibility of the alteration of polymer structure is due to the reduction in the optical band gap. [21].

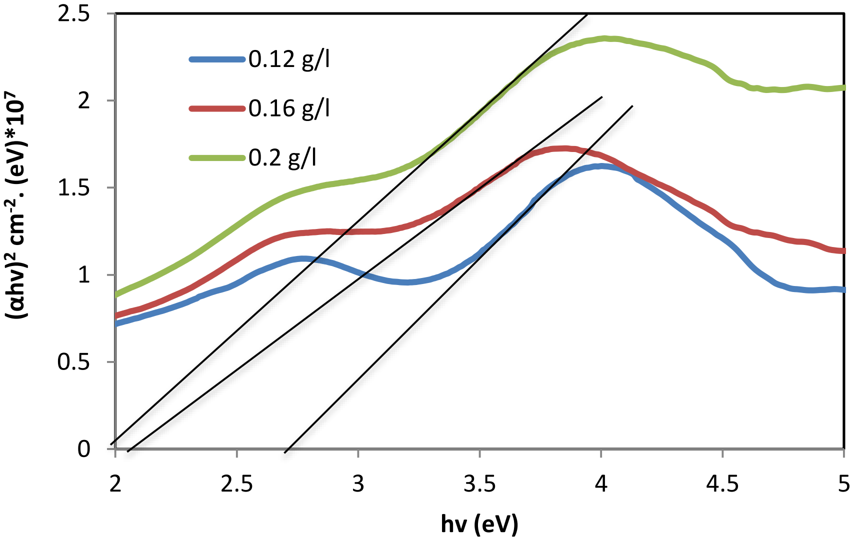

Figure 6: Direct transitional energy of polyaniline (PAni).

The index of refraction (n) is an essential optical property of polymers intricately related to other electrical and physical properties. Those who use optical methods must also investigate polymers' molecular, physical, and chemical features. The coefficient of refraction (n) is an essential optical property of polymers. As n = n + iK, n represents the real component, and k represents the imaginary component. The index of refraction, n, may be determined using the Fresnel formula given in Eq. (2) [24]:

$$\boldsymbol{n} = [\frac{\boldsymbol{4R}}{(\boldsymbol{R}-\boldsymbol{1})^2} - \boldsymbol{k}^2]^{1/2} - \frac{\boldsymbol{R}+\boldsymbol{1}}{\boldsymbol{R}-\boldsymbol{1}} \qquad \textbf{(2)}$$

Where R represents the reflectivity and k = α*λ/4*π represents the extinction coefficient. The extinction coefficient k specifies the material's features about a specific wavelength of light and displays the variations in absorption as the electromagnetic wave passes through the substance [23]. Fig. 7 exhibits the reflecting coefficient (n) values with wavelengths (λ) of PAni. The refractive coefficient decreases as the wavelength increases. The rise in the PAni Refraction coefficient at 800 nm wavelength is perhaps referred to as an increase in the packing density, a modification of the crystalline structure, and an increase in the C–H bonds with the agreed of paper [24].

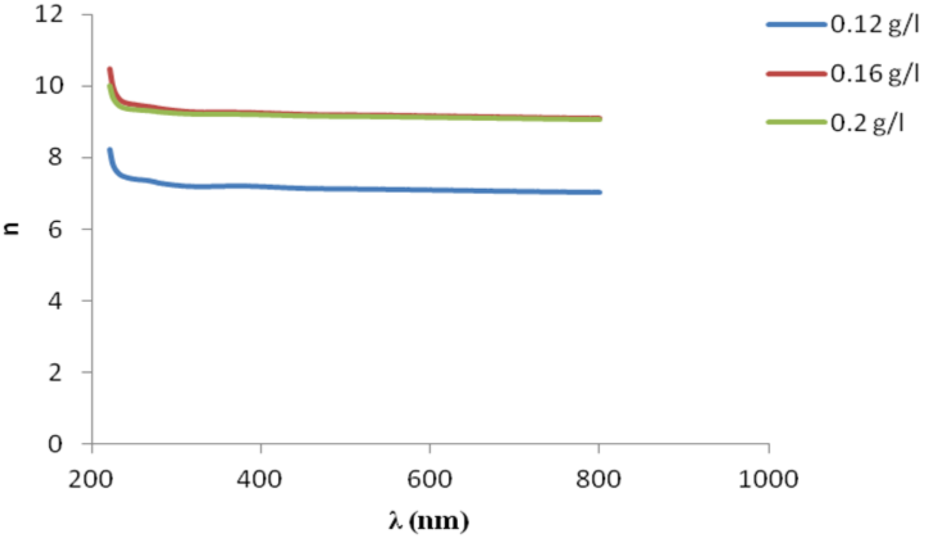

Figure 7: Polyaniline coefficient of refraction as a function of the wavelength.

Higher refractive index values represent more structural integrity. The refractive index (n) consists of a real part (r) and an imaginary part, both of which depend on the real part (r), which is part of the term that describes how much the material will slow the speed of light down. The refractive index imaginary part was found from the following relations Eq.(3) and (4) [24].

$$\varepsilon_{r=} n^2 - k^2 \qquad (3)$$

$$\varepsilon_i = 2nk \qquad (4)$$

The real part of the dielectric constant corresponds to dispersal, while the imaginary component evinces the rate of dissipation of electromagnetic wave propagation in the medium. The imaginary and real parts of the dielectric constant as a function of wavelength are manifested in Fig. 8 and 9 of PAni. The fluctuation of r is proportional to n^2 due to the modest values of K^2 relative to n^2 ($r = n^2$), but the variation of I is dependent mainly on the absorption coefficient's K value [19]. Based on Fig. 7, for the value of r at 800 nm wavelength, the reduction in optical band gap is connected to the increase in refraction coefficient. An increase in the optical dielectric constant is associated with decreasing band gaps. Also, an increase in the optical dielectric constant causes the addition of more charge carriers to the host material and, accordingly, a rise in the density of the state

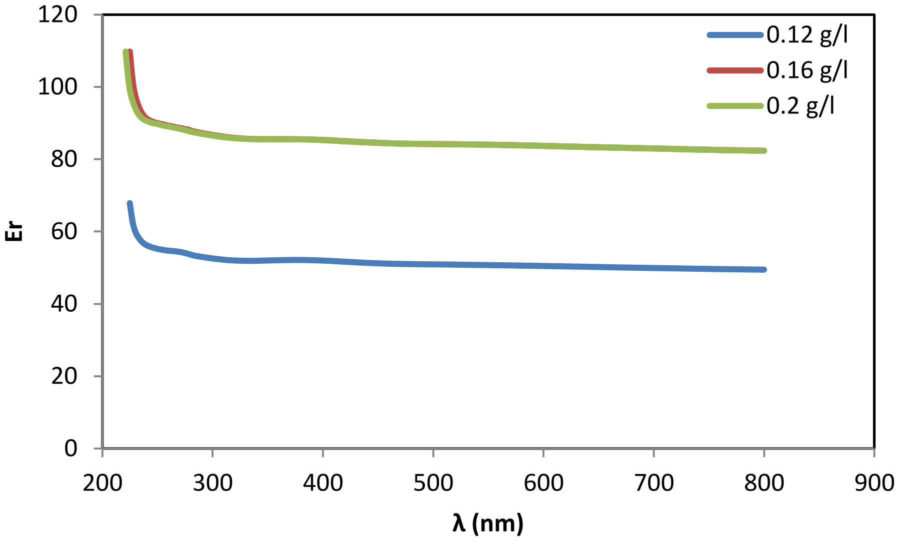

Figure 8: Pure polyaniline real dielectric constant vs wavelength.

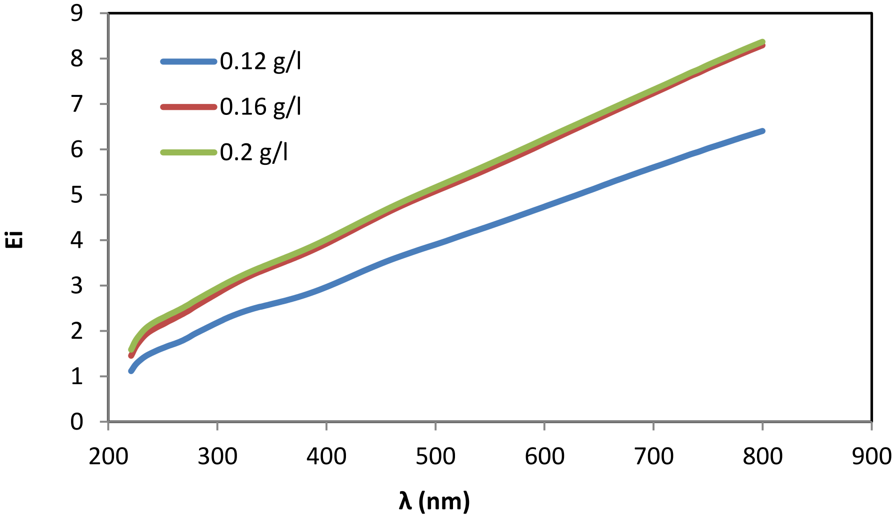

Figure 9: Pure polyaniline imaginary dielectric constant vs. wavelength.

3.5 Thermogravimetric (TGA)

The results of the TGA utilised to assess the thermal stability of the PAni sample created in this investigation are displayed in Fig. 10. Experiments were performed in hot airflow from 5°C min^{-1}. The samples lose a lot of weight in three different stages, which are, respectively, caused by the evaporation of surface-absorbed water (from room temperature to 155°C), the losses of dopant and physisorbed water (155-270°C), and the destruction and degradation of the PAni backbone (350-600°C) with agreed of paper [28]. As the synthesis temperature rose, the 20% loss of some weight temperature (T20%) and the maximum loss of some weight temperature (T_{max}) of the PAni NFs decreased instantly. T20% of PAni-0.16 g/L rose to 348°C, while T20% of PAni-0.2 g/L rose by 57°C. Furthermore, PAni-0.12 g/L had a T_{max} that was 26°C (614°C) greater than PAni-0.16 g/L. The PAni-0.12 g/L sample exhibited greater heat stability than the other samples.

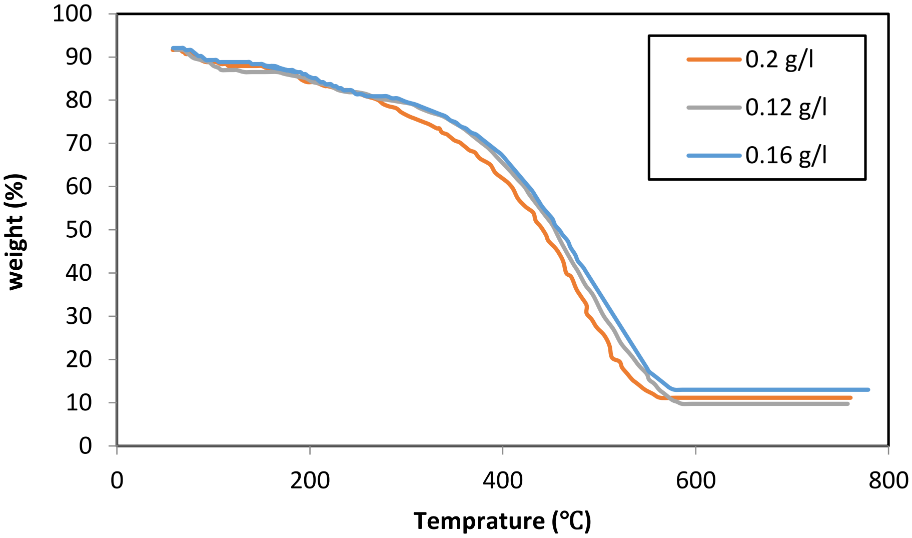

Figure 10: Thermogravimetric curves of PAni obtained at different aniline concentrations (0.12, 0.16, and 0.2 g/L).

4. Conclusions

The polymerisation of aniline has been successfully examined in the presence of different aniline concentrations. The concentration of aniline will change the shape of produced PAni Nanofibers. XRD confirmed PAni to be amorphous. FE-SEM studies revealed that the average diameter of PAni reduces with decreasing concentration. FTIR measurements demonstrated the formation of PAni at various concentrations. The optical properties elucidated that the optical band gap followed the permitted direct transition of electrons. The thermal stability for PAni-0.12 g/L was determined to be better than that of the other samples.

Conflict of Interest

The authors declare that they have no conflict of interest.

References

[1] H. Sharhan, Z. Rasheed, and J. Oleiwi, "Synthesis and Physical Characterisation of PMMA/PP and PMMA/PAN Composites for Denture Applications" *Journal of Applied Sciences and* Nanotechnology, vol. 1, no. 3, 2021.

[2] J. Chiang, and A. MacDiarmid, "Polyaniline Protonic acid doping of the emeraldine form to the metallic regime" *Synthetic Metals,* vol. 13, pp. 193-205, 1986.

[3] D. Orata, and D. Buttry, "Determination of ion populations and solvent content as functions of redox state and pH in polyaniline" *Journal of the American Chemical Society*, vol. 109, pp. 3574–3581, 1987.

[4] W. Huang, B. Humphrey, A. MacDiarmid, "Polyaniline, a novel conducting polymer. Morphology and chemistry of its oxidation and reduction in aqueous electrolytes", *Journal of the Chemical Society Faraday Transaction*, vol. 82, pp. 2385–2400, 1986.

[5] S. Golba, M. Popczyk, S. Miga, J. Jurek-Suliga, M. Zubko, "electrical conductivity and morphology study of polyaniline Powder synthesisEed with various doping ions" *Archives of Metallurgy and Materials*, vol. 64, pp. 1023-1028, 2019.

[6] C. Walkey, S. Das, S. Seal, J. Erlichman, K. Heckman, L. Ghibelli, E. Traversa, J. McGinnis, and W. Self, "Catalytic properties and biomedical applications of cerium oxide nanoparticle", *Environmental Science*", vol. 21, pp. 33–53, 2015.

[7] M. Beygisangchin, S. AbdulRashid, S. Shafie, A. Sadrolhosseini, and H. Lim, "Preparations, Properties, and Applications of Polyaniline and Polyaniline Thin Films—A Review" *Polymers (Basel)*, vol. 13, pp. 2003, 2021

[8] M. Hassen, I. Ibrahim, "Synthesis of Polyaniline–Cerium Oxide Nanocomposite for Photodetector Application*" Journal of Physics: Conference Series*. 2114, IOP 012047, 2021.

[9] A. Abdolahi, E. Hamzah, Z. Ibrahim, and S. Hashim, "Synthesis of Uniform Polyaniline Nanofibers through Interfacial Polymerization" *Materials*, vol. *5*, no. 8, pp. 1487-1494, 2012.

[10] M. Beygisangchin , S. AbdulRashid , S. Shafie , A. Sadrolhosseini , "Polyaniline Synthesised by Different Dopants for Fluorene Detection via Photoluminescence Spectroscopy" *Materials*, vol. 14, pp. 7382, 2021.

[11] L. Yue, Y. Xie, Y. Zheng, W. He, S. Guo, Y. Sun, T. Zhang, and S. Liu, "Sulfonated bacterial cellulose/ polyaniline composite membrane for use as gel polymer electrolyte" C*omposites Science and Technology*; vol. 145, pp. 122-131, 2017.

[12] F. Omar, A. Numan, N. Duraisamy, S. Bashir, K. Ramesh, and S. Ramesh , "A promising binary nanocomposite of zinc cobaltite intercalated with polyaniline for supercapacitor and hydrazine sensor" *Journal of Alloys and Compound*, vol. 716, pp. 96–105, 2017.

[13] C. Leng, J. Wei, Z. Liu, and J. Shi, "Influence of imidazolium-based ionic liquids on the performance of polyaniline/$CoFe_2O_4$ nanocomposites" *Journal of Alloys and Compound*, vol. 509, pp. 3052–3056, 2011.

[14] R. Wang, Y. Wang, C. Xu, J. Sun, and L. Gao "Facile one-step hydrazine-assisted solvothermal synthesis of nitrogen-doped reduced graphene oxide: reduction effect and mechanisms". *Journal the Royal Society of Chemistry*, vol. 3, pp. 1194–1200, 2013.

[15] C. Xu, J. Sun, and L. Gao, "Synthesis of novel hierarchical graphene/polypyrrole nanosheet composites and their superior electrochemical performance" *Journal the Royal Society of Chemistry*. vol. 21, pp. 11253–11258, 2011.

[16] V. babua, S. Vempatia, T. Uyara, and S. Ramakrishnac, "Review of one-dimensional and two-dimensional nanostructured materials for hydrogen generation" *Journal the Royal Society of Chemistry*. vol. 17, pp. 2960-2986, 2015.

[17] R. Saleh, O. Salman, and M. Dawood "Physical Investigations of Titanium Dioxide Nanorods Film Prepared by Hydrothermal Technique" *Journal of Applied Sciences and Nanotechnology*, vol. e. 1, no. 3, 2021.

[18] K. Chintala, S. Panchal, P. Rana, and R. Chauhan "Structural, optical and electrical propertie of gamma-rays exposed selenium nanowires" *Journal of Materials Science: Materials in Electronics*, vol. 27, pp. 8087–8093, 2016.

[19] T. Soliman, and A. Abouhaswa , "Synthesis and structural of $Cd_{0.5}Zn_{0.5}F_2O_4$ nanoparticles and its influence on the structure and optical properties of polyvinyl alcohol films". *Journal of Materials Science: Materials in Electronics*, vol. 31, pp. 9666–9674, 2020.

[20] P. Dipak, D. Tiwari, A. Samadhiya, N. Kumar, T. Biswajit, P. Singh, and R. Tiwari, "Synthesis of polyaniline (printable nanoink) gas sensor for the detection of ammonia gas" *Journal of Materials Science: Materials in Electronics*, vol. 31, pp. 22512–22521, 2020.

[21] S. Awad, S. El-Gamal, A. El Sayed, E. Abdel-Hady, "Characterisation, optical, and nanoscale free volume properties of Na-CMC/PAM/CNT nanocomposites" *Polymer. Advance. Technology*, vol. 31, pp. 114–125, 2020.

[22] A. Shano, and Z. Ali, "Fabrication and Characterisation of Polyaniline Nanofiber Films by Various Techniques". *Journal of Nano- and Electronic Physics*, vol. 12, no. 4, pp. 04001, 2020.

[23] Z. Ali, and A. Shano "The Influence of Solvents on Polyaniline Nanofibers Synthesised by a Hydrothermal Method and their Application in Gas Sensors" *Journal of Electronic Materials*, vol. 49, pp. 5528–5533, 2020.

[24] D. Akram, and N. Hameed "Preparation and Characterisation of PANI/PVA Blends as Electrolyte Materials" *Journal of Applied Sciences and Nanotechnology*, vol. 2, pp. 2, 2022.

[25] H. Donya, T. Taha, A. Alruwaili, I. Tomsah, and M. Ibrahim, "Micro-structure and optical spectroscopy PVA/iron oxide polymer nanocomposites" *Journal of Materials Research and Technology*, vol. 9, pp. 9189–9194, 2020.

[26] M. Ghanipour, and D. Dorranian "Effect of Ag-nanoparticles doped in polyvinyl alcohol on the structural and optical properties of PVA films" *Journal of Nanomaterials*, vol. 2013, pp. 10, 2013.

[27] C. Jin, H. Wang, Y. Liu, X. Kang, P. Liu, J. Zhang, L. Jin, S. Bian, and Q. Zhu. "High-performance yarn electrode materials enhanced by surface modifications of cotton fibers with graphene sheets and polyaniline nanowire arrays for all-solid-state supercapacitors" *Electrochimica Acta*, vol. 270, pp. 205–214, 2018.

[28] A. Sadeghi and M. Farbodi "Preparation of polyaniline–polyvinyl alcohol– silver nanocomposite and characterisation of its mechanical and antibacterial properties" *Science and Engineering Composite Materials*, vol. 25, pp. 975–982, 2018.